

Separation of chiral particles in micro- or nanofluidic channels

Sebastian Meinhardt¹, Jens Smiatek², Ralf Eichhorn³, and Friederike Schmid¹

¹ *Institut für Physik, JGU Mainz, D-55099 Mainz, Germany*

² *Institut für Physikalische Chemie, Westfälische Wilhelms-Universität Münster, D-48149 Münster, Germany*

³ *Nordita, Royal Institute of Technology and Stockholm University, Roslagstullsbacken 23, SE-106 91 Stockholm, Sweden*

We propose a method to separate enantiomers in microfluidic or nanofluidic channels. It requires flow profiles which break chiral symmetry and have regions with high local shear. Such profiles can be generated in channels confined by walls with different hydrodynamic boundary conditions (*e.g.*, slip lengths). Due to a nonlinear hydrodynamic effect, particles with different chirality migrate at different speed and can be separated. The mechanism is demonstrated by computer simulations. We investigate the influence of thermal fluctuations (*i.e.*, the Péclet number) and show that the effect disappears in the linear response regime. The details of the microscopic flow are important and determine which volume forces are necessary to achieve separation.

PACS numbers: 47.61-k, 47.61.Fg, 87.80.Qk, 87.80.Nj

Enantiomers – molecules that are not identical with their mirror image – are omnipresent in living organisms. Many biologically active molecules as well as about half of the drugs in use today are enantiomers. The pharmacological activity of drugs strongly depends on their chirality, to the point that one enantiomer may have a therapeutic effect, while its mirror image is toxic. Therefore, the separation of enantiomers by chirality is of great importance for basic science as well as for technical applications such as drug and pesticide development or in food industry^{1,2}.

In practice, chiral separation is mostly done by chemical methods, *e.g.*, by introducing chiral selector molecules in conventional separation setups such as liquid chromatography or capillary electrophoresis¹⁻³ or in miniaturized microfluidic chips^{4,5}. In recent years, however, there has been increasing interest in developing physical separation methods that do not require specific chiral recognition between molecules⁶. One of the first practical proposals due to de Gennes was to separate chiral crystals by letting them slide down an inclined plane⁷, where they would be slightly deflected from the axis of maximal slope in directions that depend on the chirality. Speer *et al.* generalized this concept of using potentials for separation and showed that chiral particles can be forced to drift in opposite directions by a combination of potentials that are periodic in time and space⁸. An alternative idea was recently put forward by Spivak and Andreev who suggested to use photoinduced drift in a gas buffer for chiral separation of small molecules⁹.

A particularly attractive approach is to use microfluidic flows for separation. The term microfluidics refers to a set of rapidly evolving technologies for preparing, controlling and analyzing minute amounts of liquids or gases, which are believed to have an enormous technological potential in many areas like pharmaceuticals, biotechnology, public health, or agriculture¹⁰. A number of suggestions have recently been made how physical properties of microfluidic flows could be exploited to separate enantiomers. Kostur *et al.* proposed to introduce flow vortices which would trap particles of different chirality at different places in space¹¹. One of us has designed a

strategy to separate enantiomers by taking advantage of different translation-rotation couplings of stereoisomers in inhomogeneous flow^{12,13}.

In these studies¹¹⁻¹³, hydrodynamic interactions were neglected. Particles were assumed to undergo Brownian motion in an externally imposed flow, without influencing the flow in return. However, hydrodynamic interactions are known to play a decisive role for the motion of microscopic particles in fluids^{14,15}. For example, chiral particles in shear flow migrate in the vorticity direction due to hydrodynamics^{16,17}. Experimentally, this effect was verified for a wide range of Reynolds numbers, ranging from macroscopic¹⁸ to the millimeter¹⁹ and micrometer scale²⁰. The direction of migration depends on the Reynolds number, but the effect itself is universal, and it has been suggested that it could be used to separate chiral particles²⁰.

In the present letter, we propose a method to achieve such a separation on the micro- and nanoscale in microfluidic channels. The main idea is to create an asymmetric flow profile with high-shear regions that drive particles of different chirality to different regions in the channel, where they migrate at different speed. This separates them while travelling through the channel. To generate asymmetric flows, we propose to exploit a particular property of micro- and nanoflows: The substrate-dependent slip at surfaces. On the macroscale, solid surfaces can usually be taken to impose "no-slip" boundary conditions on adjacent fluids, *i.e.*, the fluid particles close to the surfaces move with the same velocity as the surface. On the micro- and nanometer scale, this is not necessarily true, and particle slip may become significant, especially on hydrophobic surfaces^{21,22}: The no-slip boundary condition has to be replaced by a "partial-slip" boundary condition $\delta_B \partial_{\mathbf{n}} v_{\parallel}|_{\mathbf{r}_B} = v_{\parallel}|_{\mathbf{r}_B}$, where v_{\parallel} denotes the tangential component of the velocity and $\partial_{\mathbf{n}} v_{\parallel}$ its spatial derivative normal to the surface evaluated at the position \mathbf{r}_B of the hydrodynamic boundary. The slip length parameter δ_B depends on surface characteristics like the roughness, the hydrophobicity etc. It can be tuned, *e.g.*, by patterning the surfaces²³.

Alternatively, surface flow can be induced by electric

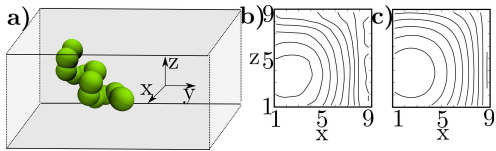


FIG. 1. Illustration of the simulation model. A helical particle moves in a square channel with asymmetric Poiseuille-like flow profile (a). Maps show the profiles across the channel: (b) DPD flow profile; (c) Corresponding theoretical profile calculated by numerical solution of the Stokes equation. The amplitudes depend on the applied pressure.

fields on charged surfaces due to an electrokinetic effect called "electroosmotic flow" (EOF)²⁴: Such surfaces are covered by a double layer of oppositely charged ions, which experience a force in an external electric field and drag the surrounding fluid along. On homogeneous surfaces, this results in an effective boundary condition $v_{\parallel} = -\mu_{\text{EOF}} E_{\parallel}$ for the flow outside the double layer, where E_{\parallel} is the tangential component of the electric field and μ_{EOF} the electroosmotic mobility. Typical values on PDMS (polydimethylsiloxane) are²⁵ $\mu_{\text{EOF}} \sim 3 \cdot 10^{-4} \text{cm}^2/\text{Vs}$. In the presence of surface slip, the magnitude of the effect can be strongly enhanced according to^{26–28} $\mu_{\text{EOF}} = -\mu_{\text{EOF}}^0 (1 + \kappa \delta_B)$, where $\kappa = \partial_{\mathbf{n}} \psi / \psi|_{\mathbf{r}_B}$ is a screening parameter describing the decay of the electrostatic potential ψ at the surface, and $\mu_{\text{EOF}}^0 = -\epsilon_r \psi(\mathbf{r}_B) / \eta_s$ the well-known Smoluchowski result²⁴ for the electroosmotic mobility at sticky walls. On patterned surfaces, the EOF behavior becomes even richer²⁹. The possibility of playing with slip lengths and surface charges by functionalizing and patterning surfaces in micro- and nanochannels enables one to adjust boundary conditions and generate asymmetric profiles^{30,31}, which could be used for chiral separation.

We first demonstrate the potential of this approach at the example of a channel with simple quadratic cross-section, whose four walls are neutral (no EOF) and have different slip lengths. We have carried out dissipative particle dynamics (DPD) simulations^{32,33} of short helical particles which are carried through such a channel by pressure-driven flow. We show that the channel indeed separates the particles effectively, and demonstrate that this is a hydrodynamic effect, which vanishes almost entirely if hydrodynamics are switched off. Finally, we discuss how the effect depends on the shear rate in the channel and the exact form of the shear profile.

The basic geometric ingredients of the simulation model are sketched in Fig. 1. In our DPD simulations, the fluid particles are transparent, *i.e.*, they interact with each other only by dissipative interactions³³. In addition, they repel the wall and the monomers of the chiral particles *via* repulsive Weeks-Chandler-Anderson (WCA) interactions³⁵. Partial slip boundary conditions are realized by introducing an additional viscous coupling with the walls. This method allows one to realize arbitrary slip lengths in a controlled manner³⁴. Specifically, the density of fluid particles in our simulations was chosen $\rho = 6\sigma^{-3}$ and the DPD friction factor $\gamma_{\text{DPD}} = 5\tau\epsilon/\sigma^2$, where the length unit σ is the DPD and WCA interaction range, the temperature unit is $\epsilon = k_B T$, and the

time unit is $\tau = \sigma\sqrt{m/\epsilon}$ with the particle mass m . The dynamic viscosity of this fluid was measured with the periodic Poiseuille flow method³⁶, giving $\eta_s = 1.35 \cdot \epsilon\tau/\sigma^3$.

The fluid is confined to a square channel with cross section $10\sigma \times 10\sigma$, which corresponds to an accessible cross section $8\sigma \times 8\sigma$ and different slip lengths at all four walls³⁷: $\delta_B^{(1)} = 11.23\sigma$, $\delta_B^{(2)} = 5.54\sigma$, $\delta_B^{(3)} = 1.58\sigma$, and $\delta_B^{(4)} = -0.17\sigma$. For pressure driven flow, this results in the profile shown in Fig. 1 (b), in good agreement with the theoretical profile obtained by direct solution of the Stokes equation (Fig. 1 c). The amplitude of the profile scales linearly with the applied pressure. At volume force $f_y = 0.1\epsilon/\sigma$, the flow velocity in the channel varies between $0.2\sigma/\tau$ and $3.6\sigma/\tau$, and the maximum shear rate in the high-shear region is $\dot{\gamma} \sim 1.0\tau^{-1}$. Mapping our model units to real SI units with a nanochannel diameter $8\sigma \sim 400\text{nm}$ and the viscosity of water $\eta_s = \eta_{\text{water}} \approx 1 \cdot 10^{-3} \text{Pa s}$ at room temperature $T = \epsilon/k_B \sim 300\text{K}$, this places τ at about $20\mu\text{s}$ and the maximum shear rate at $\dot{\gamma}_{\text{max}} \sim 0.5 \times 10^6 \text{ s}^{-1}$, a value which is experimentally accessible in nanochannels of this size³⁸. In a microchannel with diameter $10\mu\text{m}$, the same mapping gives $\tau \sim 3\text{s}$ and $\dot{\gamma}_{\text{max}} \sim 0.3\text{s}^{-1}$.

The chiral particles are represented by short helices with two windings, made of $N = 13$ spherical monomers. The helix geometry is characterized by three parameters: The radius R , the helical pitch p , and the number of monomers per turn n . Here we chose $R = 1\sigma$, $p = 3\sigma$, and $n = 6$ (see Fig. 1). This structure is stabilized by a set of stiff harmonic potentials $V(X) = k_X/2 (X - X_0)^2$, where X_0 denotes the desired value of the quantity X , and X stands for (i) the bond lengths d_i between neighbor monomers i and $i+1$, (ii) the bending angles Φ_i , (iii) the torsional angles θ_i , (iv) the distances p_j between the monomers 1, 7 and between 7, 13 (*i.e.*, the pitch), and (v) the angle Ψ between the axes of the two windings. The spring parameters were set to $k_d = k_p = 500\epsilon/\sigma^2$, $k_\phi = k_\theta = k_\Psi = 500\epsilon/\text{rad}^2$. In our model fluid, this helix had a rotational diffusion coefficient $D_R = 0.41 \cdot 10^{-2} \tau^{-1}$, a translational diffusion coefficient $D_T = 0.018\sigma^2/\tau$, and the hydrodynamic radius $R_H = k_B T / 6\pi\eta_s D_T = 2.18\sigma$.

Unless stated otherwise, the simulations were carried out at volume force $f_y = 0.1\epsilon/\sigma$ in a simulation box of length 50σ and periodic boundary conditions in the direction of flow y . The DPD time step was varied between $\delta\tau = 0.001\tau$ and $\delta\tau = 0.01\tau$ to assess and exclude finite time step artifacts.

Our central simulation result is illustrated in Fig. 2. The proposed separation strategy is clearly successful, helices of different chirality travel through the channel with different speed and can be separated along the channel (in the y direction, Fig. 2 a)). This goes along with distinctly different spatial distributions across the channel (in the (x, z) plane, Fig. 2 c)).

To assess the effect of hydrodynamic interactions, we have carried out Brownian dynamics simulations of helices moving in the tabulated flow profile $\vec{V}(\vec{r})$ of Fig. 1 b). The equation of motion for monomers i then reads $m\vec{r}_i = \vec{f}_i - \zeta(\vec{v}_i - \vec{V}(\vec{r}_i)) + \vec{\xi}_i$, where \vec{f}_i is the force acting on monomer i , \vec{v}_i its velocity, and $\vec{\xi}_i$ an uncorre-

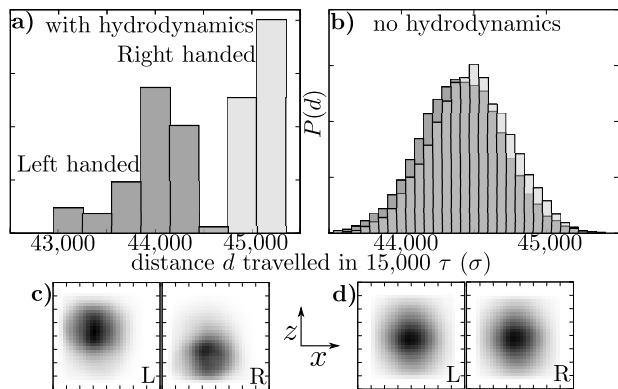


FIG. 2. Separation of chiral particles in the asymmetric channel at volume force $f_y = 0.1\epsilon/\sigma$. a) Histogram of distances travelled in the time $t = 15,000\tau$ for left handed helices (dark shaded) and right handed helices (light shaded). b) Same as a) for the Langevin simulations without hydrodynamics. c) Spatial distribution across the channel for left-handed helix (left) and right-handed helix (right) for the simulations with hydrodynamics. d) Same as c) for the Langevin simulations without hydrodynamics.

lated Gaussian white noise which satisfies the fluctuation-dissipation theorem, $\langle \xi_i^\alpha(t) \xi_j^\beta(t') \rangle = 2k_B T \zeta \delta_{ij} \delta_{\alpha\beta} \delta(t-t')$. The friction coefficient ζ was chosen such that the translational diffusion constant in the Brownian dynamics simulations matches that of the DPD simulations, *i.e.*, $\zeta = k_B T / ND_T = 4.27m/\tau$. The time step in these simulations was chosen $\delta\tau = 0.0001\tau$. The results are shown in Fig. 2 b) and d). In contrast to the results from the DPD simulations, the distributions for the two enantiomers are almost identical (Fig. 2 d)) and so are their velocities (Fig. 2 b)). Thus, the separation in the DPD simulations is driven by hydrodynamics.

The underlying mechanism, the shear-induced drift of chiral particles in the vorticity direction, is a nonlinear effect in bulk solution, which is forbidden in the linear response regime¹⁷. The shear flow must first orient the particles before it can induce drift. One would expect the separation to fail as one reaches the linear response regime. The crucial quantity in this picture is the dimensionless ratio of the shear rate $\dot{\gamma}$ and the rotational diffusion constant, the Péclet number $Pe = \dot{\gamma}/D_R$. To study this dependence on Pe in more detail, we have varied the average shear rate systematically by varying the volume force f_y on the particles. Fig. 3 a) shows the relative velocity difference between helices of different chirality as a function of f_y . As expected, it vanishes within the error for small forces. The cross-sectional distributions of the left-handed and right-handed particles approach each other continuously as one reduces the force (Fig. 3 a, inset), and separation is no longer possible. These results can be correlated with the orientation distribution of the helices. Fig. 3 b) shows that helices are mostly oriented in the flow direction. A certain amount of orientation is also observed in the simulations without hydrodynamics, probably due to the mechanisms described in Ref. 12. It accounts for the very small shift between the distance distributions for left-handed and right-handed particles in Fig. 2 b). However, the dominating effect

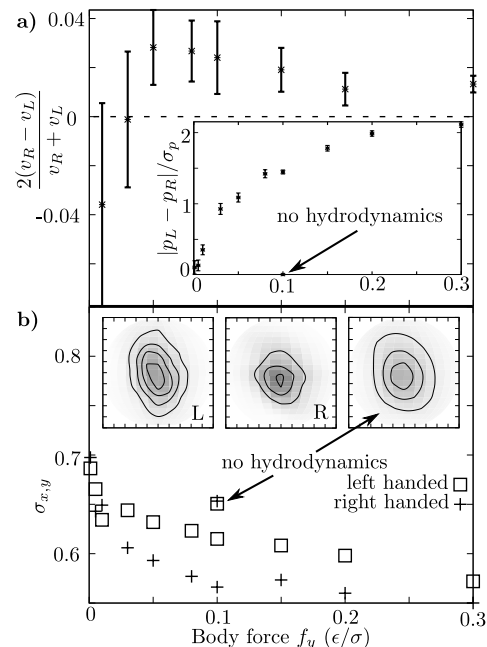


FIG. 3. Separation of chiral particles in the asymmetric channel as a function of volume force f_y . a) relative velocity difference for lefthanded and righthanded particles. Inset: distance between means of the distributions p_L and p_R for lefthanded and righthanded particles in the cross-section of the channel (the (x, z) -plane) divided by the mean standard deviation $\sigma_p = (\sigma_{p_L} + \sigma_{p_R})/2$ of the two distributions. b) Width (standard deviation) $\sigma_{x,z}$ of the distribution $P(u_x, u_z)$ of helix orientations \vec{u} projected on the (x, z) -plane. The limiting value for equidistribution on a sphere is $\sigma_{x,y} \sim 0.82$. Insets: Corresponding distributions at $f_y = 0.1\epsilon/\sigma$ for left-handed helices (L), right-handed helices (R), and helices without hydrodynamic interactions.

is clearly due to hydrodynamics. With decreasing f_y , the orientation distribution broadens until one recovers the value observed without hydrodynamics at low forces, $f_y \lesssim 0.02\epsilon/\sigma$. Taking into account that $f_y \sim 0.1\epsilon/\sigma$ corresponds to average Péclet numbers of order 120, Fig. 3 suggests that Péclet numbers of around 30 are necessary to achieve separation in our channels.

The specific threshold value depends on the details of the flow profile. For comparison, we have also studied square channels with constant shear in the x -direction by enforcing antiparallel fluid velocities at the opposing (y, z) -boundaries. Technically, such channels can be realized by inducing EOF of different amplitudes on two opposing sides of the channel combined with full-slip boundary conditions on the remaining two sides. Since they have symmetric flow profiles, they will not propel chiral particles with distinct (average) migration velocities and thus cannot be used to separate particles in the y direction along the channel. Particles of different chirality migrate at equal speed in contrast to the asymmetric profiles discussed above, but they may still occupy different regions in the (x, z) -plane, and this effect also depends on the Péclet number as shown in Fig. 4. As one increases the Péclet number, the distributions of left-handed and right-handed particles in the (x, z) -plane move apart. This sets in at much earlier Péclet numbers than in the asymmetric channel ($Pe \sim 0.5$). However, a

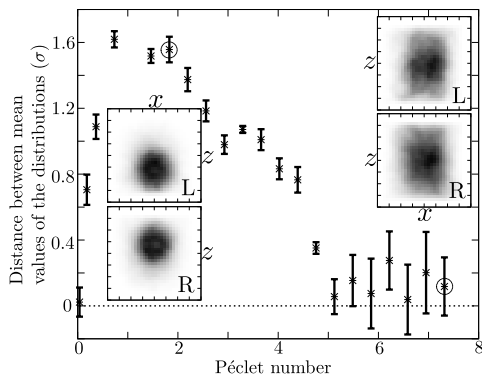


FIG. 4. Spatial separation of chiral particles in a symmetric square channel with constant shear in x -direction as a function of Péclet number. The insets show explicit distributions at the encircled values.

second effect comes into play at higher Péclet numbers, which causes the distributions to move together again and merge again at $Pe \sim 5$. The reasons for this unex-

pected behavior are not yet clear. Most likely, it is due to the onset of inertial effects at higher Reynolds numbers Re , which push the Helices towards the center of the channel³⁹. This effect should thus disappear in real nano- or microchannels, where Re is small, whereas it is of order $Re \sim 10$ in our DPD simulations.

To summarize, we have demonstrated that it is possible to separate enantiomers on microscopic scales in asymmetric flows without explicit chiral agents. By comparing simulations with and without hydrodynamic interactions, we have shown that the separation is dominated by hydrodynamic mechanisms. They can be exploited to force particles of different chirality into different regions of the channel where they migrate at different speed. We have demonstrated the effect for simple, not optimized, square geometries, and we have shown that it is highly susceptible to the flow profile. Other (e.g., rectangular) channel geometries can presumably be designed where the separation will be even more efficient.

This work was funded in part by the VW foundation and the German Science Foundation within SFB-TR6. We thank Peter Reimann for useful discussions.

- ¹ J.E. Rekoske, *AIChE Journal* **47**, 2 (2001).
- ² G. Gübitz and M.G. Schmid, *Mol. Biotech.* **32**, 159 (2006).
- ³ T.J. Ward and B.A. Baker **80**, 4363 (2008).
- ⁴ D. Belder and M. Ludwig, *Electrophoresis* **24**, 2422 (2003).
- ⁵ S. Nagl, P. Schulze, M. Ludwig, D. Belder, *Electrophoresis* **30**, 2765 (2009).
- ⁶ C.J. Welch, *Enantiomer* **3**, 275 (1998).
- ⁷ P.G. de Gennes, *Europhys. Lett.* **46**, 827 (1999).
- ⁸ D. Speer, R. Eichhorn, and P. Reimann, *Phys. Rev. Lett.* **105**, 090602 (2010).
- ⁹ B. Spivak and A.V. Andreev, *Phys. Rev. Lett.* **102**, 063004 (2009).
- ¹⁰ J. Ouellette, *The Industrial Physicist* **9**, 14 (2003).
- ¹¹ M. Kostur, M. Schindler, P. Talkner, P. Hänggi, *Phys. Rev. Lett.* **96**, 014502 (2006).
- ¹² R. Eichhorn, *Phys. Rev. Lett.* **105**, 034502 (2010).
- ¹³ R. Eichhorn, *Chem. Phys.* **375**, 568 (2010).
- ¹⁴ J.K.G. Dhont, *An Introduction to Dynamics of Colloids* (Elsevier, Amsterdam, 1996).
- ¹⁵ J. Happel, H. Brenner, *Low Reynolds number hydrodynamics* (Kluwer, Dordrecht, 1983).
- ¹⁶ Y.-J. Kim and W.J. Rai, *Int. J. Multiphase Flow* **17**, 717 (1991).
- ¹⁷ M. Makino and M. Doi, *Phys. Fluids* **17**, 103605 (2005).
- ¹⁸ P. Chen and C.-H. Chao, *Phys. Fluids* **19**, 017108 (2007).
- ¹⁹ M. Makino, L. Arai, and M. Doi, *J. Phys. Soc. Jpn.* **77**, 064404 (2008).
- ²⁰ Marcos, H.C. Fu, T.R. Powers, R. Stocker, *Phys. Rev. Lett.* **102**, 158103 (2009).
- ²¹ R. Pit, H. Hervet, and L. Leger, *Phys. Rev. Lett.* **85**, 980 (2000).
- ²² C. Neto, D.R. Evans, E. Bonaccorso, H.-J. Butt, V.S.J. Craig, *Rep. Prog. Phys.* **68**, 2859 (2005).
- ²³ P. Joseph, C. Cottin-Bizonne, J.-M. Benoit, C. Ybert, C. Journet, P. Tabeling, L. Bocquet, *Phys. Rev. Lett.* **97**, 156104 (2006).
- ²⁴ R.J. Hunter, *Foundations of Colloid Science* (Clarendon press, Oxford, 1991).
- ²⁵ M. Streek, F. Schmid, T.T. Duong, D. Anselmetti, A. Ros, *Phys. Rev. E* **71**, 011905 (2005).
- ²⁶ V.M. Muller, I.P. Sergeeva, V.D. Sobolev, N.V. Churaev, *Kolloidnyi Zhurnal* **48**, 718 (1984); *Colloid J. USSR* **48**, 606 (1986).
- ²⁷ C.I. Bouzigues, P. Tabeling, and L. Bocquet, *Phys. Rev. Lett.* **101**, 114503 (2008).
- ²⁸ J. Smiatek and F. Schmid, *J. Phys. Chem. B* **114**, 6266 (2010).
- ²⁹ A.V. Belyaev and O.I. Vinogradova, *Phys. Rev. Lett.* **107**, 098301 (2011).
- ³⁰ L. Bogunovic, C. Vosskötter, and D. Anselmetti, preprint (2012).
- ³¹ When exploiting EOF, one must ensure that the chiral particles are not attracted by the charged walls and that the channel diameter is large compared to the thickness of the charged double layer. (~ 1 nm in physiological buffers).
- ³² P.J. Hoogerbrugge and J.M. Koelman, *Europhys. Lett.* **19**, 155 (1992).
- ³³ P. Espanol and P. Warren, *Europhys. Lett.* **30**, 191 (1995).
- ³⁴ J. Smiatek, M.P. Allen, and F. Schmid, *Eur. Phys. J. E* **26**, 115 (2008).
- ³⁵ J.D. Weeks, D. Chandler, and H.D. Andersen, *J. Chem. Phys.* **54**, 5237 (1971).
- ³⁶ J.A. Backer, C.P. Lowe, H.C.J. Hoefsloot, P. D. Iedema, *J. Chem. Phys.* **122**, 154503 (2005).
- ³⁷ Even though the effective slip length is negative, the fluid velocities in the surface region are of course always positive.
- ³⁸ C. Kuang and G. Wang, *Lab Chip* **10**, 240 (2010).
- ³⁹ D. Di Carlo, J.F. Edd, K.J. Humphry, H.A. Stone, M. Toner, *Phys. Rev. Lett.* **102**, 094503 (2009).